

Study of $B^{\pm,0} \rightarrow J/\psi K^+ K^- K^{\pm,0}$ and search for $B^0 \rightarrow J/\psi \phi$ at BABAR

J. P. Lees,¹ V. Poireau,¹ V. Tisserand,¹ E. Grauges,² A. Palano,^{3a,3b} G. Eigen,⁴ B. Stugu,⁴ D. N. Brown,⁵ L. T. Kerth,⁵ Yu. G. Kolomensky,⁵ M. J. Lee,⁵ G. Lynch,⁵ H. Koch,⁶ T. Schroeder,⁶ C. Hearty,⁷ T. S. Mattison,⁷ J. A. McKenna,⁷ R. Y. So,⁷ A. Khan,⁸ V. E. Blinov,^{9a,9c} A. R. Buzykaev,^{9a} V. P. Druzhinin,^{9a,9b} V. B. Golubev,^{9a,9b} E. A. Kravchenko,^{9a,9b} A. P. Onuchin,^{9a,9c} S. I. Serednyakov,^{9a,9b} Yu. I. Skovpen,^{9a,9b} E. P. Solodov,^{9a,9b} K. Yu. Todyshev,^{9a,9b} A. N. Yushkov,^{9a} A. J. Lankford,¹⁰ M. Mandelkern,¹⁰ B. Dey,¹¹ J. W. Gary,¹¹ O. Long,¹¹ C. Campagnari,¹² M. Franco Sevilla,¹² T. M. Hong,¹² D. Kovalskiy,¹² J. D. Richman,¹² C. A. West,¹² A. M. Eisner,¹³ W. S. Lockman,¹³ W. Panduro Vazquez,¹³ B. A. Schumm,¹³ A. Seiden,¹³ D. S. Chao,¹⁴ C. H. Cheng,¹⁴ B. Echenard,¹⁴ K. T. Flood,¹⁴ D. G. Hitlin,¹⁴ T. S. Miyashita,¹⁴ P. Ongmongkolkul,¹⁴ F. C. Porter,¹⁴ R. Andreassen,¹⁵ Z. Huard,¹⁵ B. T. Meadows,¹⁵ B. G. Pushpawela,¹⁵ M. D. Sokoloff,¹⁵ L. Sun,¹⁵ P. C. Bloom,¹⁶ W. T. Ford,¹⁶ A. Gaz,¹⁶ U. Nauenberg,¹⁶ J. G. Smith,¹⁶ S. R. Wagner,¹⁶ R. Ayad,^{17,†} W. H. Toki,¹⁷ B. Spaan,¹⁸ R. Schwierz,¹⁹ D. Bernard,²⁰ M. Verderi,²⁰ S. Playfer,²¹ D. Bettoni,^{22a} C. Bozzi,^{22a} R. Calabrese,^{22a,22b} G. Cibinetto,^{22a,22b} E. Fioravanti,^{22a,22b} I. Garzia,^{22a,22b} E. Luppi,^{22a,22b} L. Piemontese,^{22a} V. Santoro,^{22a} A. Calcaterra,²³ R. de Sangro,²³ G. Finocchiaro,²³ S. Martellotti,²³ P. Patteri,²³ I. M. Peruzzi,^{23,‡} M. Piccolo,²³ M. Rama,²³ A. Zallo,²³ R. Contri,^{24a,24b} E. Guido,^{24a,24b} M. Lo Vetere,^{24a,24b} M. R. Monge,^{24a,24b} S. Passaggio,^{24a} C. Patrignani,^{24a,24b} E. Robutti,^{24a} B. Bhuyan,²⁵ V. Prasad,²⁵ M. Morii,²⁶ A. Adametz,²⁷ U. Uwer,²⁷ H. M. Lacker,²⁸ P. D. Dauncey,²⁹ U. Mallik,³⁰ C. Chen,³¹ J. Cochran,³¹ W. T. Meyer,³¹ S. Prell,³¹ H. Ahmed,³² A. V. Gritsan,³³ N. Arnaud,³⁴ M. Davier,³⁴ D. Derkach,³⁴ G. Grosdidier,³⁴ F. Le Diberder,³⁴ A. M. Lutz,³⁴ B. Malaescu,^{34,§} P. Roudeau,³⁴ A. Stocchi,³⁴ G. Wormser,³⁴ D. J. Lange,³⁵ D. M. Wright,³⁵ J. P. Coleman,³⁶ J. R. Fry,³⁶ E. Gabathuler,³⁶ D. E. Hutchcroft,³⁶ D. J. Payne,³⁶ C. Touramanis,³⁶ A. J. Bevan,³⁷ F. Di Lodovico,³⁷ R. Sacco,³⁷ G. Cowan,³⁸ J. Bougher,³⁹ D. N. Brown,³⁹ C. L. Davis,³⁹ A. G. Denig,⁴⁰ M. Fritsch,⁴⁰ W. Gradl,⁴⁰ K. Griessinger,⁴⁰ A. Hafner,⁴⁰ E. Prencipe,^{40,||} K. R. Schubert,⁴⁰ R. J. Barlow,^{41,¶} G. D. Lafferty,⁴¹ R. Cenci,⁴² B. Hamilton,⁴² A. Jawahery,⁴² D. A. Roberts,⁴² R. Cowan,⁴³ D. Dujmic,⁴³ G. Sciolla,⁴³ R. Cheaib,⁴⁴ P. M. Patel,^{44,*} S. H. Robertson,⁴⁴ P. Biassoni,^{45a,45b} N. Neri,^{45a} F. Palombo,^{45a,45b} L. Cremaldi,⁴⁶ R. Godang,^{46,**} P. Sonnek,⁴⁶ D. J. Summers,⁴⁶ M. Simard,⁴⁷ P. Taras,⁴⁷ G. De Nardo,^{48a,48b} D. Monorchio,^{48a,48b} G. Onorato,^{48a,48b} C. Sciacca,^{48a,48b} M. Martinelli,⁴⁹ G. Raven,⁴⁹ C. P. Jessop,⁵⁰ J. M. LoSecco,⁵⁰ K. Honscheid,⁵¹ R. Kass,⁵¹ J. Brau,⁵² R. Frey,⁵² N. B. Sinev,⁵² D. Strom,⁵² E. Torrence,⁵² E. Feltres,^{53a,53b} M. Margoni,^{53a,53b} M. Morandin,^{53a} M. Posocco,^{53a} M. Rotondo,^{53a} G. Simi,^{53a,53b} F. Simonetto,^{53a,53b} R. Stroili,^{53a,53b} S. Akar,⁵⁴ E. Ben-Haim,⁵⁴ M. Bomben,⁵⁴ G. R. Bonneaud,⁵⁴ H. Briand,⁵⁴ G. Calderini,⁵⁴ J. Chauveau,⁵⁴ Ph. Leruste,⁵⁴ G. Marchiori,⁵⁴ J. Ocariz,⁵⁴ S. Sitt,⁵⁴ M. Biasini,^{55a,55b} E. Manoni,^{55a} S. Pacetti,^{55a,55b} A. Rossi,^{55a} C. Angelini,^{56a,56b} G. Batignani,^{56a,56b} S. Bettarini,^{56a,56b} M. Carpinelli,^{56a,56b,††} G. Casarosa,^{56a,56b} A. Cervelli,^{56a,56b} M. Chrzaszcz,^{56a,56b} F. Forti,^{56a,56b} M. A. Giorgi,^{56a,56b} A. Lusiani,^{56a,56c} B. Oberhof,^{56a,56b} E. Paoloni,^{56a,56b} A. Perez,^{56a} G. Rizzo,^{56a,56b} J. J. Walsh,^{56a} D. Lopes Pegna,⁵⁷ J. Olsen,⁵⁷ A. J. S. Smith,⁵⁷ R. Faccini,^{58a,58b} F. Ferrarotto,^{58a} F. Ferroni,^{58a,58b} M. Gaspero,^{58a,58b} L. Li Gioi,^{58a} G. Piredda,^{58a} C. Büniger,⁵⁹ S. Dittrich,⁵⁹ O. Grünberg,⁵⁹ T. Hartmann,⁵⁹ T. Leddig,⁵⁹ C. Voß,⁵⁹ R. Waldi,⁵⁹ T. Adye,⁶⁰ E. O. Olaiya,⁶⁰ F. F. Wilson,⁶⁰ S. Emery,⁶¹ G. Vasseur,⁶¹ F. Anulli,^{62,‡‡} D. Aston,⁶² D. J. Bard,⁶² J. F. Benitez,⁶² C. Cartaro,⁶² M. R. Convery,⁶² J. Dorfan,⁶² G. P. Dubois-Felsmann,⁶² W. Dunwoodie,⁶² M. Ebert,⁶² R. C. Field,⁶² B. G. Fulsom,⁶² A. M. Gabareen,⁶² M. T. Graham,⁶² C. Hast,⁶² W. R. Innes,⁶² P. Kim,⁶² M. L. Kocian,⁶² D. W. G. S. Leith,⁶² P. Lewis,⁶² D. Lindemann,⁶² B. Lindquist,⁶² S. Luitz,⁶² V. Luth,⁶² H. L. Lynch,⁶² D. B. MacFarlane,⁶² D. R. Muller,⁶² H. Neal,⁶² S. Nelson,⁶² M. Perl,⁶² T. Pulliam,⁶² B. N. Ratcliff,⁶² A. Roodman,⁶² A. A. Salnikov,⁶² R. H. Schindler,⁶² A. Snyder,⁶² D. Su,⁶² M. K. Sullivan,⁶² J. Va'vra,⁶² A. P. Wagner,⁶² W. F. Wang,⁶² W. J. Wisniewski,⁶² M. Wittgen,⁶² D. H. Wright,⁶² H. W. Wulsin,⁶² V. Ziegler,⁶² M. V. Purohit,⁶³ R. M. White,^{63,§§} J. R. Wilson,⁶³ A. Randle-Conde,⁶⁴ S. J. Sekula,⁶⁴ M. Bellis,⁶⁵ P. R. Burchat,⁶⁵ E. M. T. Puccio,⁶⁵ M. S. Alam,⁶⁶ J. A. Ernst,⁶⁶ R. Gorodeisky,⁶⁷ N. Guttman,⁶⁷ D. R. Peimer,⁶⁷ A. Soffer,⁶⁷ S. M. Spanier,⁶⁸ J. L. Ritchie,⁶⁹ A. M. Ruland,⁶⁹ R. F. Schwitters,⁶⁹ B. C. Wray,⁶⁹ J. M. Izen,⁷⁰ X. C. Lou,⁷⁰ F. Bianchi,^{71a,71b} F. De Mori,^{71a,71b} A. Filippi,^{71a} D. Gamba,^{71a,71b} S. Zambito,^{71a,71b} L. Lanceri,^{71a,71b} L. Vitale,^{72a,72b} F. Martinez-Vidal,⁷³ A. Oyanguren,⁷³ P. Villanueva-Perez,⁷³ J. Albert,⁷⁴ Sw. Banerjee,⁷⁴ F. U. Bernlochner,⁷⁴ H. H. F. Choi,⁷⁴ G. J. King,⁷⁴ R. Kowalewski,⁷⁴ M. J. Lewczuk,⁷⁴ T. Lueck,⁷⁴ I. M. Nugent,⁷⁴ J. M. Roney,⁷⁴ R. J. Sobie,⁷⁴ N. Tasneem,⁷⁴ T. J. Gershon,⁷⁵ P. F. Harrison,⁷⁵ T. E. Latham,⁷⁵ H. R. Band,⁷⁶ S. Dasu,⁷⁶ Y. Pan,⁷⁶ R. Prepost,⁷⁶ and S. L. Wu⁷⁶

(BABAR Collaboration)

¹Laboratoire d'Annecy-le-Vieux de Physique des Particules (LAPP), Université de Savoie, CNRS/IN2P3, F-74941 Annecy-Le-Vieux, France²Universitat de Barcelona, Facultat de Física, Departament ECM, E-08028 Barcelona, Spain^{3a}INFN Sezione di Bari, I-70126 Bari, Italy;^{3b}Dipartimento di Fisica, Università di Bari, I-70126 Bari, Italy⁴University of Bergen, Institute of Physics, N-5007 Bergen, Norway

- ⁵Lawrence Berkeley National Laboratory and University of California, Berkeley, California 94720, USA
- ⁶Ruhr Universität Bochum, Institut für Experimentalphysik 1, D-44780 Bochum, Germany
- ⁷University of British Columbia, Vancouver, British Columbia V6T 1Z1, Canada
- ⁸Brunel University, Uxbridge, Middlesex UB8 3PH, United Kingdom
- ^{9a}Budker Institute of Nuclear Physics SB RAS, Novosibirsk 630090, Russia;
- ^{9b}Novosibirsk State University, Novosibirsk 630090, Russia
- ^{9c}Novosibirsk State Technical University, Novosibirsk 630092, Russia
- ¹⁰University of California at Irvine, Irvine, California 92697, USA
- ¹¹University of California at Riverside, Riverside, California 92521, USA
- ¹²University of California at Santa Barbara, Santa Barbara, California 93106, USA
- ¹³University of California at Santa Cruz, Institute for Particle Physics, Santa Cruz, California 95064, USA
- ¹⁴California Institute of Technology, Pasadena, California 91125, USA
- ¹⁵University of Cincinnati, Cincinnati, Ohio 45221, USA
- ¹⁶University of Colorado, Boulder, Colorado 80309, USA
- ¹⁷Colorado State University, Fort Collins, Colorado 80523, USA
- ¹⁸Technische Universität Dortmund, Fakultät Physik, D-44221 Dortmund, Germany
- ¹⁹Technische Universität Dresden, Institut für Kern- und Teilchenphysik, D-01062 Dresden, Germany
- ²⁰Laboratoire Leprince-Ringuet, Ecole Polytechnique, CNRS/IN2P3, F-91128 Palaiseau, France
- ²¹University of Edinburgh, Edinburgh EH9 3JZ, United Kingdom
- ^{22a}INFN Sezione di Ferrara, I-44122 Ferrara, Italy
- ^{22b}Dipartimento di Fisica e Scienze della Terra, Università di Ferrara, I-44122 Ferrara, Italy
- ²³INFN Laboratori Nazionali di Frascati, I-00044 Frascati, Italy
- ^{24a}INFN Sezione di Genova, I-16146 Genova, Italy
- ^{24a}Dipartimento di Fisica, Università di Genova, I-16146 Genova, Italy
- ²⁵Indian Institute of Technology Guwahati, Guwahati, Assam, 781 039, India
- ²⁶Harvard University, Cambridge, Massachusetts 02138, USA
- ²⁷Universität Heidelberg, Physikalisches Institut, D-69120 Heidelberg, Germany
- ²⁸Humboldt-Universität zu Berlin, Institut für Physik, D-12489 Berlin, Germany
- ²⁹Imperial College London, London SW7 2AZ, United Kingdom
- ³⁰University of Iowa, Iowa City, Iowa 52242, USA
- ³¹Iowa State University, Ames, Iowa 50011-3160, USA
- ³²Physics Department, Jazan University, Jazan 22822, Kingdom of Saudi Arabia
- ³³Johns Hopkins University, Baltimore, Maryland 21218, USA
- ³⁴Laboratoire de l'Accélérateur Linéaire, IN2P3/CNRS et Université Paris-Sud 11, Centre Scientifique d'Orsay, F-91898 Orsay Cedex, France
- ³⁵Lawrence Livermore National Laboratory, Livermore, California 94550, USA
- ³⁶University of Liverpool, Liverpool L69 7ZE, United Kingdom
- ³⁷Queen Mary, University of London, London E1 4NS, United Kingdom
- ³⁸University of London, Royal Holloway and Bedford New College, Egham, Surrey TW20 0EX, United Kingdom
- ³⁹University of Louisville, Louisville, Kentucky 40292, USA
- ⁴⁰Johannes Gutenberg-Universität Mainz, Institut für Kernphysik, D-55099 Mainz, Germany
- ⁴¹University of Manchester, Manchester M13 9PL, United Kingdom
- ⁴²University of Maryland, College Park, Maryland 20742, USA
- ⁴³Massachusetts Institute of Technology, Laboratory for Nuclear Science, Cambridge, Massachusetts 02139, USA
- ⁴⁴McGill University, Montréal, Québec H3A 2T8, Canada
- ^{45a}INFN Sezione di Milano, I-20133 Milano, Italy;
- ^{45b}Dipartimento di Fisica, Università di Milano, I-20133 Milano, Italy
- ⁴⁶University of Mississippi, University, Mississippi 38677, USA
- ⁴⁷Université de Montréal, Physique des Particules, Montréal, Québec H3C 3J7, Canada
- ^{48a}INFN Sezione di Napoli, I-80126 Napoli, Italy;
- ^{48b}Dipartimento di Scienze Fisiche, Università di Napoli Federico II, I-80126 Napoli, Italy
- ⁴⁹NIKHEF, National Institute for Nuclear Physics and High Energy Physics, NL-1009 DB Amsterdam, Netherlands
- ⁵⁰University of Notre Dame, Notre Dame, Indiana 46556, USA
- ⁵¹Ohio State University, Columbus, Ohio 43210, USA
- ⁵²University of Oregon, Eugene, Oregon 97403, USA
- ^{53a}INFN Sezione di Padova, I-35131 Padova, Italy
- ^{53b}Dipartimento di Fisica, Università di Padova, I-35131 Padova, Italy

⁵⁴Laboratoire de Physique Nucléaire et de Hautes Energies, IN2P3/CNRS, Université Pierre et Marie Curie-Paris 6, Université Denis Diderot-Paris7, F-75252 Paris, France

^{55a}INFN Sezione di Perugia, I-06123 Perugia, Italy

^{55b}Dipartimento di Fisica, Università di Perugia, I-06123 Perugia, Italy

^{56a}INFN Sezione di Pisa, I-56127 Pisa, Italy

^{56b}Dipartimento di Fisica, Università di Pisa, I-56127 Pisa, Italy

^{56c}Scuola Normale Superiore di Pisa, I-56127 Pisa, Italy

⁵⁷Princeton University, Princeton, New Jersey 08544, USA

^{58a}INFN Sezione di Roma, I-00185 Roma, Italy

^{58b}Dipartimento di Fisica, Università di Roma La Sapienza, I-00185 Roma, Italy

⁵⁹Universität Rostock, D-18051 Rostock, Germany

⁶⁰Rutherford Appleton Laboratory, Chilton, Didcot, Oxon OX11 0QX, United Kingdom

⁶¹CEA, Irfu, SPP, Centre de Saclay, F-91191 Gif-sur-Yvette, France

⁶²SLAC National Accelerator Laboratory, Stanford, California 94309 USA

⁶³University of South Carolina, Columbia, South Carolina 29208, USA

⁶⁴Southern Methodist University, Dallas, Texas 75275, USA

⁶⁵Stanford University, Stanford, California 94305-4060, USA

⁶⁶State University of New York, Albany, New York 12222, USA

⁶⁷Tel Aviv University, School of Physics and Astronomy, Tel Aviv 69978, Israel

⁶⁸University of Tennessee, Knoxville, Tennessee 37996, USA

⁶⁹University of Texas at Austin, Austin, Texas 78712, USA

⁷⁰University of Texas at Dallas, Richardson, Texas 75083, USA

^{71a}INFN Sezione di Torino, I-10125 Torino, Italy

^{71b}Dipartimento di Fisica, Università di Torino, I-10125 Torino, Italy

^{72a}INFN Sezione di Trieste, I-34127 Trieste, Italy

^{72b}Dipartimento di Fisica, Università di Trieste, I-34127 Trieste, Italy

⁷³IFIC, Universitat de Valencia-CSIC, E-46071 Valencia, Spain

⁷⁴University of Victoria, Victoria, British Columbia V8W 3P6, Canada

⁷⁵Department of Physics, University of Warwick, Coventry CV4 7AL, United Kingdom

⁷⁶University of Wisconsin, Madison, Wisconsin 53706, USA

(Received 31 July 2014; published 7 January 2015)

We study the rare B meson decays $B^{\pm,0} \rightarrow J/\psi K^+ K^- K^{\pm,0}$, $B^{\pm,0} \rightarrow J/\psi \phi K^{\pm,0}$, and search for $B^0 \rightarrow J/\psi \phi$, using 469×10^6 $B\bar{B}$ events collected at the $\Upsilon(4S)$ resonance with the BABAR detector at the PEP-II e^+e^- asymmetric energy collider. We present new measurements of branching fractions and a study of the $J/\psi \phi$ mass distribution in search of new charmonium-like states. In addition, we search for the decay $B^0 \rightarrow J/\psi \phi$ and find no evidence of a signal.

DOI: 10.1103/PhysRevD.91.012003

PACS numbers: 13.25.Hw, 12.15.Hh, 11.30.Er

I. INTRODUCTION

Many charmonium-like resonances have been discovered in the past, revealing a spectrum too rich to interpret in terms of conventional mesons expected from potential models [1]. In several cases, it has not been possible to assign a spin-parity value to the resonance. Some of them have been extensively investigated as possible candidates for nonconventional mesons, such as tetraquarks, glueballs, or hybrids [2].

In a search for exotic states, the CDF experiment studied the decay $B^+ \rightarrow J/\psi \phi K^+$ [3], where $J/\psi \rightarrow \mu^+ \mu^-$ and $\phi(1020) \rightarrow K^+ K^-$, claiming the observation of a resonance labeled the $X(4140)$ decaying to $J/\psi \phi$ [4]. They found evidence in the same decay mode for another resonance, labeled as the $X(4270)$ [5]. Recently, the LHCb experiment studied the decay $B^+ \rightarrow J/\psi \phi K^+$ in pp collisions at 7 TeV, with a data sample more than 3

*Deceased.

†Present address: University of Tabuk, Tabuk 71491, Saudi Arabia.

‡Also at Università di Perugia, Dipartimento di Fisica, Perugia, Italy.

§Present address: Laboratoire de Physique Nucléaire et de Hautes Energies, IN2P3/CNRS, Paris, France.

||Present address: Forschungszentrum Jülich GmbH, D-52425 Jülich, Germany.

¶Present address: University of Huddersfield, Huddersfield HD1 3DH, United Kingdom.

**Present address: University of South Alabama, Mobile, Alabama 36688, USA.

††Also at Università di Sassari, Sassari, Italy.

‡‡Also at INFN Sezione di Roma, Roma, Italy.

§§Present address: Universidad Técnica Federico Santa María, Valparaíso 2390123, Chile.

times larger than that of CDF, and set an upper limit (UL) incompatible with the CDF result [6]. The D0 and the CMS experiments more recently made studies of the same decay channel, leading to different conclusions [7,8] than the LHCb experiment. In this work we study the rare decays $B^+ \rightarrow J/\psi K^+ K^- K^+$, $B^0 \rightarrow J/\psi K^+ K^- K_S^0$ and search for possible resonant states in the $J/\psi\phi$ mass spectrum. We also search for the decay $B^0 \rightarrow J/\psi\phi$, which is expected to proceed mainly via a Cabibbo-suppressed and color-suppressed transition $\bar{b}d \rightarrow \bar{c}c\bar{d}$. The absence of a signal would indicate that the required rescattering of $\bar{d}d$ into $\bar{s}s$ is very small.

This paper is organized as follows: in Sec. II we describe the detector and data selection, and in Sec. III we report the branching-fraction (BF) measurements. Section IV is devoted to the resonance search, while Sec. V summarizes the results.

II. THE BABAR DETECTOR AND DATA SELECTION

We make use of the data set collected by the BABAR detector at the PEP-II e^+e^- storage rings operating at the $\Upsilon(4S)$ resonance. The integrated luminosity for this analysis is 422.5 fb^{-1} , which corresponds to the production of $469 \times 10^6 \text{ } B\bar{B}$ pairs [9].

The BABAR detector is described in detail elsewhere [10]. We mention here only the components of the detector that are used in the present analysis. Charged particles are detected and their momenta measured with a combination of a cylindrical drift chamber (DCH) and a silicon vertex tracker (SVT), both operating within the 1.5 T magnetic field of a superconducting solenoid. Information from a ring-imaging Cherenkov detector (DIRC) is combined with specific ionization measurements from the SVT and DCH to identify charged kaon and pion candidates. The efficiency for kaon identification is 90%, while the rate for a pion being misidentified as a kaon is 2%. For low-transverse-momentum kaon candidates that do not reach the DIRC, particle identification relies only on the energy loss measurement, so that the transverse momentum spectrum of identified kaons extends down to $150 \text{ MeV}/c$. Electrons are identified using information provided by a CsI(Tl) electromagnetic calorimeter (EMC), in combination with that from the SVT and DCH, while muons are identified in the Instrumented Flux Return (IFR). This is the outermost subdetector, in which muon/pion discrimination is performed. Photons are detected, and their energies measured with the EMC.

For each signal event candidate, we first reconstruct the J/ψ by geometrically constraining to a common vertex a pair of oppositely charged tracks, identified as either electrons or muons, and apply a loose requirement that the χ^2 fit probability exceed 0.1%. For $J/\psi \rightarrow e^+e^-$ we use bremsstrahlung energy-loss recovery: if an electron-associated photon cluster is found in the EMC, its

three-momentum vector is incorporated into the calculation of the invariant mass $m_{e^+e^-}$. The vertex fit for a J/ψ candidate includes a constraint to the nominal J/ψ mass value [11].

For $B^+ \rightarrow J/\psi K^+ K^- K^+$ candidates, we combine the J/ψ candidate with three loosely identified kaons and require a vertex-fit probability larger than 0.1%. Similarly, for $B^0 \rightarrow J/\psi K^- K^+ K_S^0$ candidates, we combine the J/ψ and K_S^0 with two loosely identified kaons and require a vertex-fit probability larger than 0.1%.

A K_S^0 candidate is formed by geometrically constraining a pair of oppositely charged tracks to a common vertex, with χ^2 fit probability larger than 0.1%. The pion mass is assigned to the tracks without particle identification (PID) requirements. The three-momenta of the two pions are then added and the K_S^0 energy is computed using the nominal K_S^0 mass. We require the K_S^0 flight length significance with respect to the B^0 vertex to be larger than 3σ .

We further select B meson candidates using the energy difference $\Delta E \equiv E_B^* - \sqrt{s}/2$ in the center-of-mass frame and the beam-energy-substituted mass defined as $m_{\text{ES}} \equiv \sqrt{((s/2 + \vec{p}_i \cdot \vec{p}_B)/E_i)^2 - \vec{p}_B^2}$, where (E_i, \vec{p}_i) is the initial-state e^+e^- four-momentum vector in the laboratory frame and \sqrt{s} is the center-of-mass energy. In the above expressions E_B^* is the B meson candidate energy in the center-of-mass frame, and \vec{p}_B is its laboratory frame momentum.

When multiple candidates are present, the combination with the smallest ΔE is chosen. We find that, after requiring $m_{\text{ES}} > 5.2 \text{ GeV}/c^2$, the fraction of events having multiple candidates is 1.3% for B^+ and 8.6% for B^0 . From simulation, we find that 99.6% of the time we choose the correct candidate.

The final selection requires $|\Delta E| < 30 \text{ MeV}$ and $|\Delta E| < 25 \text{ MeV}$ for B^+ and B^0 decays, respectively; the additional selection criterion $m_{\text{ES}} > 5.2 \text{ GeV}/c^2$ is required for the calculation of the BFs, while $m_{\text{ES}} > 5.27 \text{ GeV}/c^2$ is applied to select the signal region for the analysis of the invariant mass systems.

III. BRANCHING FRACTIONS

Figure 1 shows the m_{ES} distributions for (a) $B^+ \rightarrow J/\psi K^+ K^- K^+$ and (b) $B^0 \rightarrow J/\psi K^- K^+ K_S^0$ candidates after having applied the ΔE selections described in Sec. II, while the corresponding ΔE distributions are shown in Figs. 1(c) and 1(d), respectively, for $m_{\text{ES}} > 5.27 \text{ GeV}/c^2$. Figure 2 shows the K^+K^- invariant mass distribution in the region $m_{K^+K^-} < 1.1 \text{ GeV}/c^2$ for (a) B^+ and (b) B^0 candidates. A clean $\phi(1020)$ signal is present in both mass spectra. The background contributions, estimated from the ΔE sidebands in the range $40 < |\Delta E| < 70 \text{ MeV}$, are shown as shaded histograms in Figs. 2(a) and 2(b) and are seen to be small. In the following we have ignored the presence of possible additional S-wave contributions in the $\phi(1020)$ signal region.

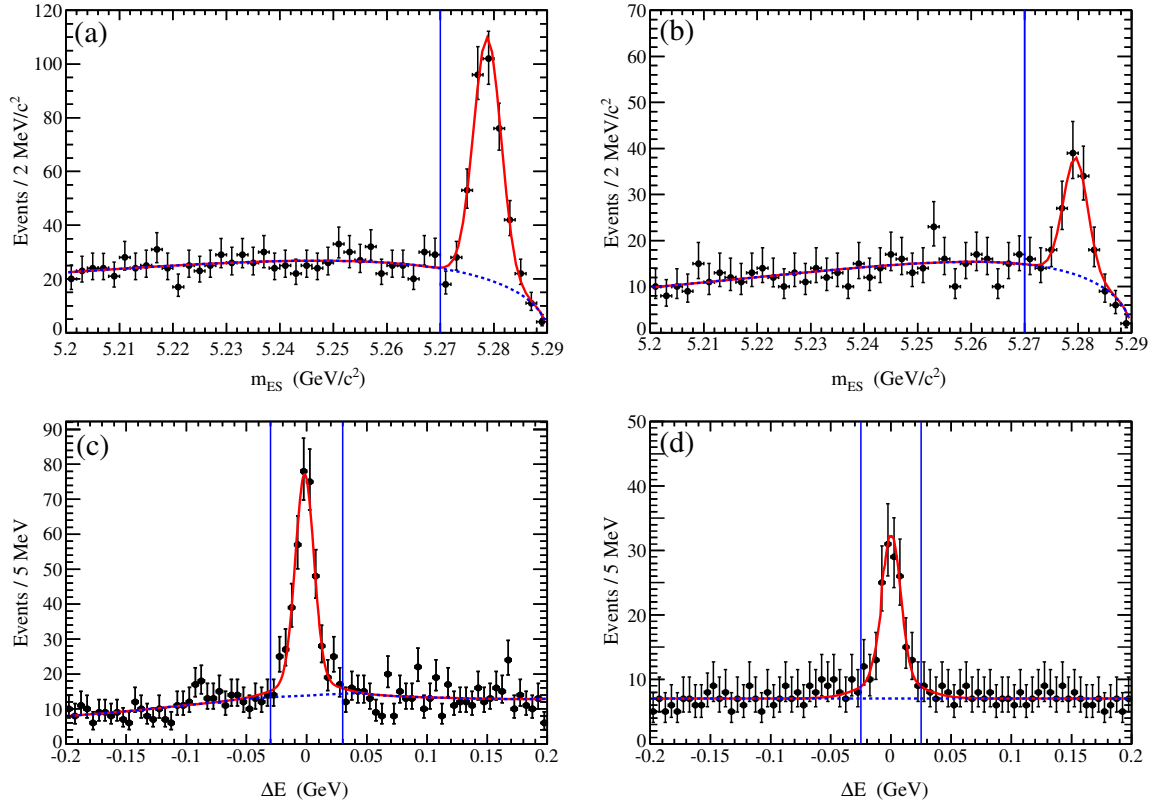


FIG. 1 (color online). The m_{ES} distributions for (a) $B^+ \rightarrow J/\psi K^+ K^- K^+$ and (b) $B^0 \rightarrow J/\psi K^- K^+ K_S^0$, for the ΔE regions indicated in the text. The ΔE distributions for $m_{ES} > 5.27 \text{ GeV}/c^2$ are shown for (c) $B^+ \rightarrow J/\psi K^+ K^- K^+$ and (d) $B^0 \rightarrow J/\psi K^- K^+ K_S^0$. The continuous (red) curve represents the signal plus background, while the dotted (blue) curve represents the fitted background. Vertical (blue) lines indicate the selected signal regions.

We select the $\phi(1020)$ signal region to be in the mass range $[1.004\text{--}1.034] \text{ GeV}/c^2$. Figure 2 shows the m_{ES} distribution for (c) $B^+ \rightarrow J/\psi \phi K^+$ and (d) $B^0 \rightarrow J/\psi \phi K_S^0$ candidates, respectively, for events in the ϕ mass region, which satisfy the ΔE selection criteria. Figures 2(e) and 2(f) show the ΔE distribution for $m_{ES} > 5.27 \text{ GeV}/c^2$, when requiring the $K^+ K^-$ invariant mass to be in the $\phi(1020)$ signal region. The distributions of Figs. 2(c) and 2(e) contain 212 events in the m_{ES} and ΔE signal region, with an estimated background of 23 events. Similarly, those of Figs. 2(d) and 2(f) contain 50 events, with an estimated background of 9 events.

We search for the decay $B^0 \rightarrow J/\psi \phi$ by constraining a fitted J/ψ and two loosely identified kaon candidates to a common vertex. Possible backgrounds originating from the decay $B^0 \rightarrow J/\psi K^{0*}(892)$, $K^{0*}(892) \rightarrow K^- \pi^+$, and from the channel $B^0 \rightarrow J/\psi K_1(1270)$, $K_1(1270) \rightarrow K^- \pi^+ \pi^0$, are found to be consistent with zero, after applying a dedicated selection as described in Secs. II and III. Figure 3 shows the corresponding m_{ES} and ΔE distributions. We do not observe a significant signal for this decay mode.

For Figs. 1–3 an unbinned maximum likelihood fit to each m_{ES} distribution is performed to determine the yield and obtain a BF measurement [12]. We use the sum of two

functions to parametrize the m_{ES} distribution; a Gaussian function describes the signal, and an ARGUS function [13] the background. A study of the ΔE sidebands did not show the presence of peaking backgrounds. Table I summarizes the fitted yields obtained.

As a validation test, we fit the ΔE distributions shown in Figs. 1–3, using a double-Gaussian model for the signal and a linear function for the background, and we obtain yields consistent with those from the m_{ES} fits.

The signals in Fig. 1, corresponding to the $B^+ \rightarrow J/\psi K^+ K^- K^+$ and the $B^0 \rightarrow J/\psi K^- K^+ K_S^0$ decays, yield 14.4σ and 5.5σ significance, respectively. Those in Fig. 2, which restrict the invariant mass $m_{K^+ K^-}$ to the signal region of the $\phi(1020)$ meson, are observed with significance 16.1σ and 5.6σ , respectively. In this paper the statistical significance of the peaks is evaluated as $\sqrt{-2 \ln(L_0/L_{\max})}$, where L_{\max} and L_0 represent the maximum likelihood values with the fitted signal yield and with the signal yield fixed to zero, respectively.

We estimate the efficiency for the different channels using Monte Carlo (MC) simulations. For each channel we perform full detector simulations where B mesons decay uniformly over the available phase space (PHSP). These simulated events are then reconstructed and analyzed, as

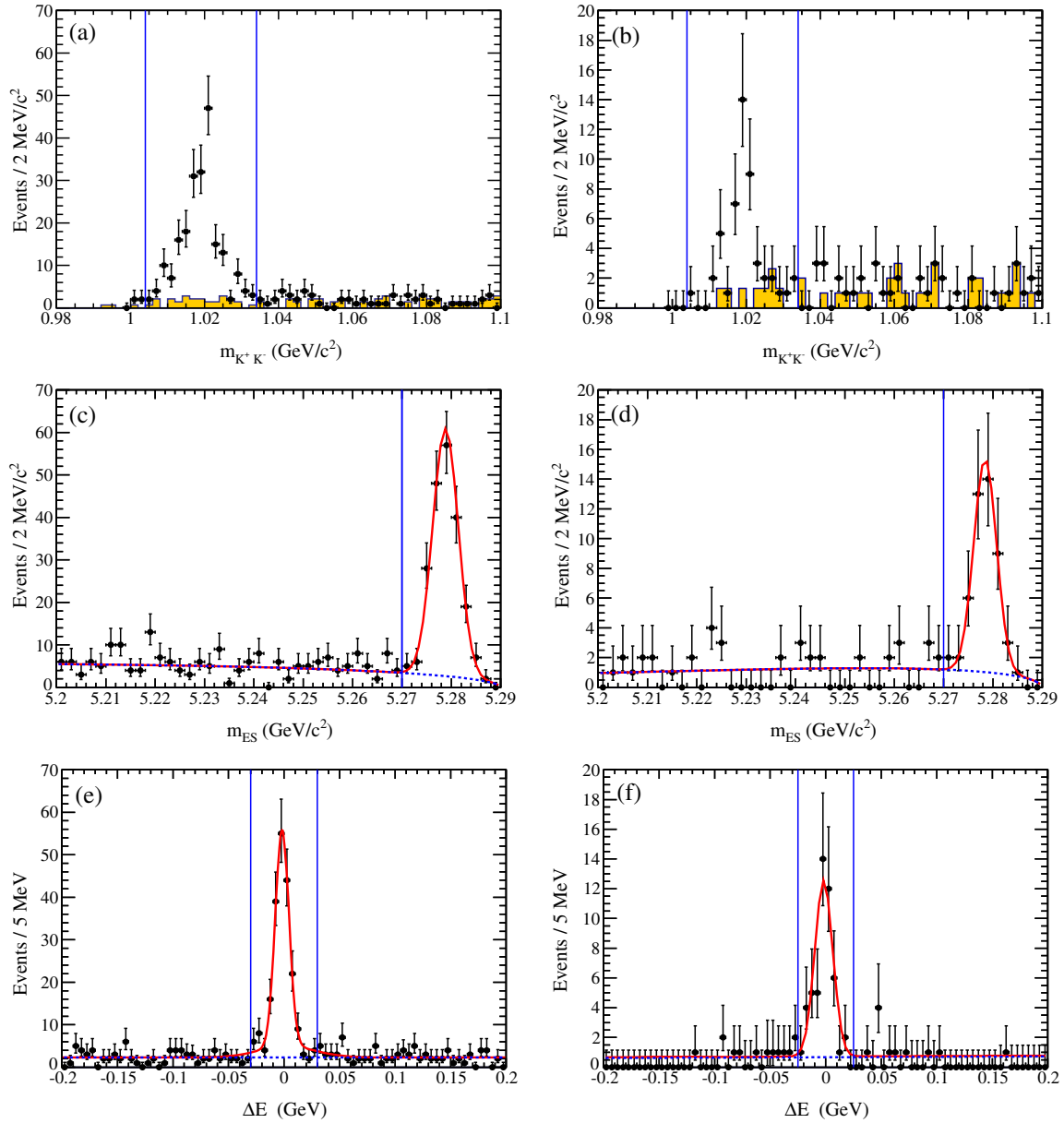


FIG. 2 (color online). (a) The K^+K^- mass spectrum, (c) m_{ES} , and (e) ΔE distribution for $B^+ \rightarrow J/\psi\phi K^+$. (b) The K^+K^- mass spectrum, (d) m_{ES} , and (f) ΔE distribution for $B^0 \rightarrow J/\psi\phi K_S^0$. The dots are the data points, and the shaded (yellow) distributions are obtained from the ΔE sidebands. Vertical (blue) lines indicate the selected signal regions. In (a) and (b) the m_{ES} and ΔE selection criteria described in Sec. II have been applied.

are the real data. These MC simulations are also used to validate the analysis procedure and the BF extractions.

Table I reports the resulting integrated efficiencies for the different channels, and the efficiency-corrected yields. The efficiency is computed in two different ways. For $B^+ \rightarrow J/\psi\phi K^+$ and $B^0 \rightarrow J/\psi\phi K_S^0$ we make use of a Dalitz-plot-dependent efficiency, where each event is weighted by the inverse of the efficiency evaluated in the appropriate cell of the Dalitz plot shown in Fig. 4. This approach is particularly important because of the lower efficiency observed at low $J/\psi\phi$ invariant mass, where the spectrum deviates from pure PHSP behavior. For the ϕ channels, the

“Corrected yield” values in Table I are obtained as sums of inverse Dalitz-plot efficiencies for events in the ϕ signal regions with background subtraction taken into account as described in Sec. IV. The events in the ϕ signal region account for about 65% of the data in the four-body final states. There is no evidence of structure in the remaining $\sim 35\%$ of these events, and so they are corrected according to their average efficiency obtained from MC simulation of four-body PHSP samples. For these channels, $B^+ \rightarrow J/\psi K^+ K^- K^+$ and $B^0 \rightarrow J/\psi K^+ K^- K_S^0$, the PHSP corrected yield is added to the ϕ signal region corrected yield to obtain the “Corrected yield” values in lines 1 and 3 of

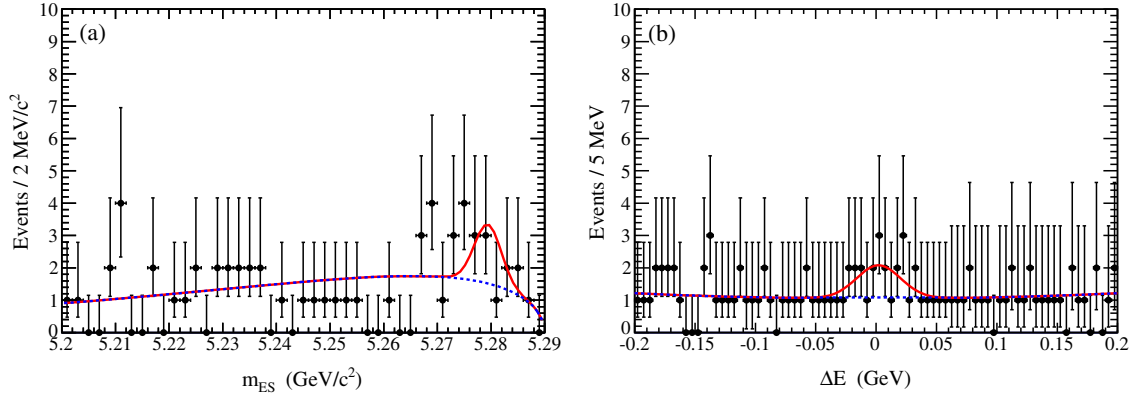


FIG. 3 (color online). (a) The m_{ES} and (b) ΔE distribution for $B^0 \rightarrow J/\psi\phi$ event candidates. The curves in (a) and (b) are the result of the fits described in the text.

Table I. The efficiency values in the third column of Table I correspond to “Event yield” divided by “Corrected yield.”

Systematic uncertainties affecting the BF measurements are listed in Table II. The evaluation of the integrated luminosity is performed using the method of $B\bar{B}$ counting [10], and we assign a uniform 0.6% uncertainty to all the final states. The uncertainty on the efficiency evaluation related to the size of the MC simulations is negligible with respect to the other contributions. The systematic uncertainty on the reconstruction efficiency of charged-particle tracks is estimated from the comparison of data samples and full detector simulations for well-chosen decay modes. In a similar way we obtain a 1.7% systematic uncertainty in the reconstruction of K_S^0 meson decays. In the case of the $B^0 \rightarrow J/\psi\phi K_S^0$ and $B^+ \rightarrow J/\psi\phi K^+$ decay modes, since the J/ψ and the ϕ are vector states, we compute the efficiency also under the assumption that the two vector mesons are transversely or longitudinally polarized. We consider the uncertainties related to the choice of the probability density functions (pdf) in the fit procedure, by varying fixed parameters by $\pm 1\sigma$ in their uncertainties. We also evaluate the efficiency variations for different charged-particle-track PID. All uncertainties are added in quadrature. We note that the BF for $B^+ \rightarrow J/\psi\phi K^+$ and that for $B^0 \rightarrow J/\psi\phi K^0$ are in agreement with their previous *BABAR* measurements [14], which already dominate the PDG average values [11], but now we obtain more than 4 times better precision. The combination of these decay

modes was observed first by the CLEO Collaboration [15]. Our BF value for the decay $B^+ \rightarrow J/\psi K^+ K^- K^+$ is the first measurement. For the decay $B^0 \rightarrow J/\psi K^+ K^- K^0$, the LHCb Collaboration has obtained a BF value $(2.02 \pm 0.43 \pm 0.17 \pm 0.08) \times 10^{-5}$ [16], which is consistent with our result.

We estimate an upper limit (UL) at a 90% confidence level (C.L.) for the BF of the decay $B^0 \rightarrow J/\psi\phi$. The signal yield obtained from the fit to the m_{ES} distribution is 6 ± 4 events [Fig. 3(a)], corresponding to an UL at 90% C.L. of 14 events. The Feldman-Cousins method [17] is used to evaluate ULs on BFs. Ensembles of pseudoexperiments are generated according to the pdfs for a given signal yield (10000 sets of signal and background events), and fits are performed. We obtain an UL on the $B^0 \rightarrow J/\psi\phi$ BF of 1.01×10^{-6} . The Belle Collaboration reported a limit of 0.94×10^{-6} [18], while a recent analysis from the LHCb Collaboration lowers this limit to 1.9×10^{-7} [19].

We compute the ratios

$$R_+ = \frac{\mathcal{B}(B^+ \rightarrow J/\psi K^+ K^- K^+)}{\mathcal{B}(B^+ \rightarrow J/\psi\phi K^+)} = 0.67 \pm 0.07 \pm 0.03 \quad (1)$$

and

$$R_0 = \frac{\mathcal{B}(B^0 \rightarrow J/\psi K^+ K^- K^0)}{\mathcal{B}(B^0 \rightarrow J/\psi\phi K^0)} = 0.79 \pm 0.20 \pm 0.05, \quad (2)$$

TABLE I. Event yields, efficiencies (ϵ) and BF measurements (\mathcal{B}) for the different decay modes. For channels involving K_S^0 , the yields and efficiencies refer to $K_S^0 \rightarrow \pi^+\pi^-$, and the BF includes the corrections for $K_S^0 \rightarrow \pi^0\pi^0$ and K_L^0 decay. The $B^0 \rightarrow J/\psi\phi$ UL at a 90% C.L. is listed at the end of the table.

B channel	Event yield	ϵ (%)	Corrected yield	$\mathcal{B} (\times 10^{-5})$
$B^+ \rightarrow J/\psi K^+ K^- K^+$	290 ± 22	15.08 ± 0.04	1923 ± 146	$3.37 \pm 0.25 \pm 0.14$
$B^+ \rightarrow J/\psi\phi K^+$	189 ± 14	13.54 ± 0.04	1396 ± 103	$5.00 \pm 0.37 \pm 0.15$
$B^0 \rightarrow J/\psi K^+ K^- K^0$	68 ± 13	10.35 ± 0.04	657 ± 126	$3.49 \pm 0.67 \pm 0.15$
$B^0 \rightarrow J/\psi\phi K^0$	41 ± 7	10.10 ± 0.04	406 ± 69	$4.43 \pm 0.76 \pm 0.19$
$B^0 \rightarrow J/\psi\phi$	6 ± 4	31.12 ± 0.07	19 ± 13	< 0.101

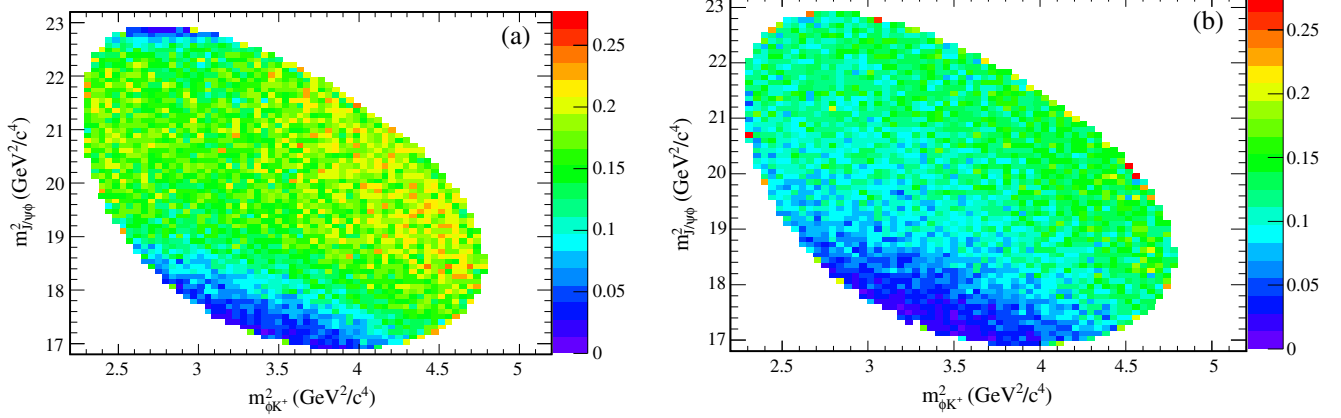


FIG. 4 (color online). Efficiency distribution on the Dalitz plot for (a) $B^+ \rightarrow J/\psi\phi K^+$ and (b) $B^0 \rightarrow J/\psi\phi K_S^0$.

and they are consistent with being equal within the uncertainties. We also compute the ratios

$$R_\phi = \frac{\mathcal{B}(B^0 \rightarrow J/\psi\phi K^0)}{\mathcal{B}(B^+ \rightarrow J/\psi\phi K^+)} = 0.89 \pm 0.17 \pm 0.04 \quad (3)$$

and

$$R_{2K} = \frac{\mathcal{B}(B^0 \rightarrow J/\psi K^+ K^- K^0)}{\mathcal{B}(B^+ \rightarrow J/\psi K^+ K^- K^+)} = 1.04 \pm 0.21 \pm 0.06. \quad (4)$$

On the basis of the simplest relevant color-suppressed spectator quark model diagrams (e.g. Fig. 1 of Ref. [15]), it would be expected that $R_+ = R_0$ and $R_\phi \sim R_{2K} \sim 1$. Our measured values of these ratios are consistent with these expectations.

IV. SEARCH FOR RESONANCE PRODUCTION

We plot in Fig. 5(a) the $J/\psi K^+ K^-$ mass distribution for $B^+ \rightarrow J/\psi K^+ K^- K^+$ and in Fig. 5(b) that for $B^0 \rightarrow J/\psi K^- K^+ K_S^0$; the signal regions are defined by the ΔE selections indicated in Sec. II and $m_{ES} > 5.27 \text{ GeV}/c^2$. No prominent structure is observed in both mass spectra.

We select events in the ϕ signal regions and search for the resonant states reported by the CDF Collaboration in the $J/\psi\phi$ mass spectrum [5]. The mass and the width values are fixed to $m = 4143.4 \text{ MeV}/c^2$ and $\Gamma = 15.3 \text{ MeV}$ for the $X(4140)$, and to $m = 4274.4 \text{ MeV}/c^2$ and $\Gamma = 32.3 \text{ MeV}$ for the $X(4270)$ resonance. We evaluate the mass resolution using MC simulations and obtain $2 \text{ MeV}/c^2$ resolution in the mass region between $4100 \text{ MeV}/c^2$ and $4300 \text{ MeV}/c^2$. Therefore, resolution effects can be ignored because they are much smaller than the widths of the resonances under consideration.

We estimate the efficiency on each quasi-three-body Dalitz plot as the ratio between the reconstructed and generated distributions, where the values are generated according to PHSP. Figure 4 shows the resulting distributions evaluated over the $m^2_{J/\psi\phi}$ versus $m^2_{\phi K}$ plane for the charged (a) and neutral (b) B decay, respectively. The lower efficiency at low $J/\psi\phi$ mass is due to the lower reconstruction efficiency for low kaon momentum in the laboratory frame, as a result of energy loss in the beampipe and SVT material.

We test the agreement between data and MC by using a full MC simulation where the $B^+ \rightarrow J/\psi\phi K^+$ and $B^0 \rightarrow J/\psi\phi K_S^0$ decays are included with known branching fractions. We repeat the entire analysis on these simulated

TABLE II. Systematic uncertainty contributions (%) to the evaluation of the BFs.

Source	$B^+ \rightarrow J/\psi K^+ K^- K^+$	$B^+ \rightarrow J/\psi\phi K^+$	$B^0 \rightarrow J/\psi K^- K^+ K_S^0$	$B^0 \rightarrow J/\psi\phi K_S^0$	$B^0 \rightarrow J/\psi\phi$
$B\bar{B}$ counting	0.6	0.6	0.6	0.6	0.6
Efficiency	0.04	0.04	0.04	0.04	0.07
Tracking	0.9	0.9	1.2	1.2	0.7
K_S^0	1.7	1.7	...
Secondary BFs	0.08	0.5	0.1	0.5	0.5
Decay model	...	0.4	...	0.9	1.0
pdfs	3.0	0.7	2.0	0.5	1.0
PID	2.5	2.5	3.0	3.0	2.0
Total contribution	4.1	3.0	4.2	4.4	2.7

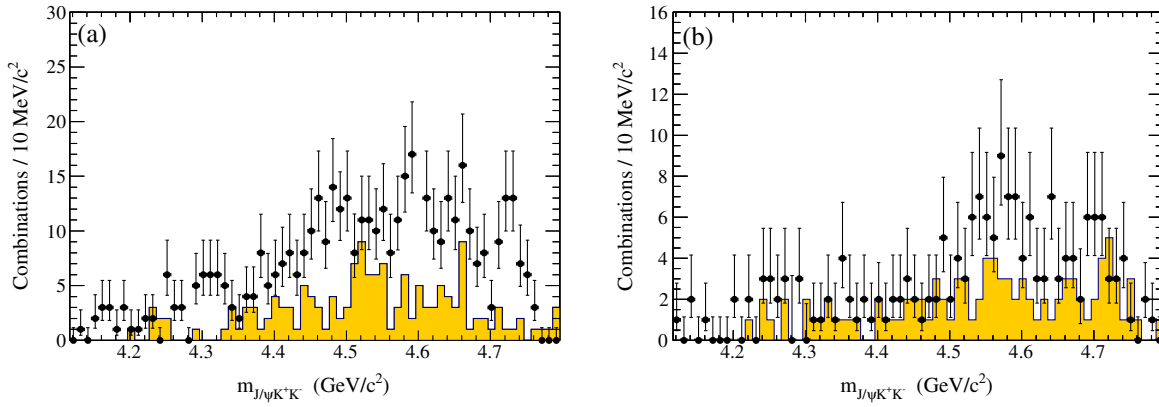


FIG. 5 (color online). Invariant mass distribution $J/\psi K^+ K^-$ for (a) $B^+ \rightarrow J/\psi K^+ K^- K^+$ and (b) $B^0 \rightarrow J/\psi K^+ K^- K_S^0$. The shaded (yellow) histogram on each figure indicates the background estimated from the ΔE sidebands.

data and find good agreement between generated and reconstructed branching fractions. Resolution effects are small and are computed using MC simulations. We obtain average values of 2.9 MeV for $(J/\psi\phi)$ and 2.2 MeV for $(J/\psi K)$. These small values do not produce bias in the evaluation of the efficiency and the measurement of the branching fractions.

To search for the two resonances in the $J/\psi\phi$ mass distributions, we perform unbinned maximum likelihood fits to the $B \rightarrow J/\psi\phi K$ decay Dalitz plots. We model the resonances using S-wave relativistic Breit-Wigner (BW) functions with parameters fixed to the CDF values. The nonresonant contributions are represented by a constant term, and no interference is allowed between the fit components. We estimate the background contributions from the ΔE sidebands, find them to be small and consistent with a PHSP behavior, and so in the fits they are incorporated into the nonresonant PHSP term. The decay of a pseudoscalar meson to two vector states may contain high spin contributions which could generate nonuniform angular distributions. However, due to the limited data sample we do not include such angular terms, and we assume that the resonances decay isotropically. The amplitudes are normalized using PHSP MC-generated

events with B parameters obtained from the fits to the data. The fit functions are weighted by the two-dimensional efficiency computed on the Dalitz plots.

We perform fits separately for the charged B^+ sample and the combined B^+ and B^0 samples. Due to the very limited statistics of the B^0 sample we do not perform a separate fit, but instead subtract the fit result for the B^+ sample from that for the combined B^+ and B^0 sample. In this case we make use of the two different efficiencies for the two channels. In the MC simulation performed, we make use of a weighted mean of the two efficiencies evaluated on the respective Dalitz plots.

Table III summarizes the results of the fits. We report the background-corrected fit fractions for the two resonances, $f_{X(4140)}$ and $f_{X(4270)}$, the two-dimensional (2D) χ^2 computed on the Dalitz plot, and the one-dimensional (1D) χ^2 computed on the $J/\psi\phi$ mass projection. For this purpose, we use an adaptive binning method and divide the Dalitz plot into a number of cells in such a way that the minimum expected population per cell is not smaller than 7. We generate MC simulations weighted by the efficiency and by the results from the fits. These are normalized to the event yield in data, using the same bin definitions. We then compute the $\chi^2 = \sum_{i=1}^{N_{\text{cells}}} (N_{\text{obs}}^i - N_{\text{exp}}^i)^2 / N_{\text{exp}}^i$, where N_{obs}^i

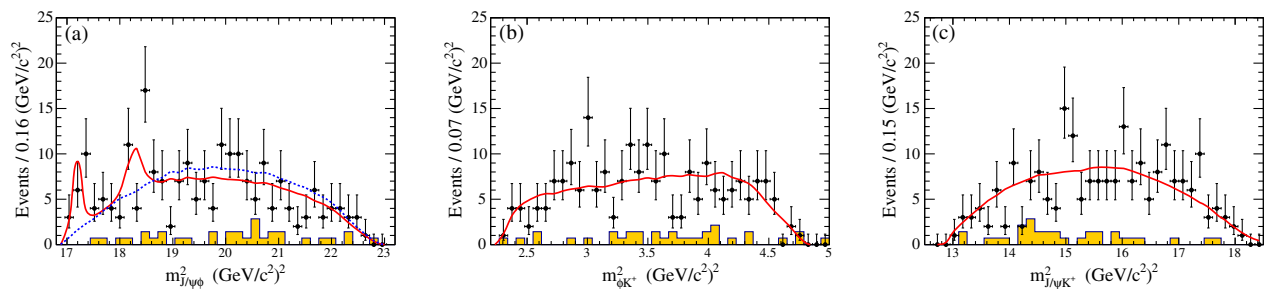


FIG. 6 (color online). Dalitz plot projections for $B^+ \rightarrow J/\psi\phi K^+$ on (a) $m_{J/\psi\phi}^2$, (b) $m_{\phi K^+}^2$, and (c) $m_{J/\psi K^+}^2$. The continuous (red) curves are the results from fit model A performed including the $X(4140)$ and $X(4270)$ resonances. The dashed (blue) curve in (a) indicates the projection for fit model D, with no resonances. The shaded (yellow) histograms indicate the background estimated from the ΔE sidebands.

TABLE III. Results of the fits to the $B \rightarrow J/\psi\phi K$ Dalitz plots. For each fit, the table gives the fit fraction for each resonance, and the 2D and 1D χ^2 values. The fractions are corrected for the background component.

Channel	Fit	$f_{X(4140)}$ (%)	$f_{X(4270)}$ (%)	2D χ^2/ν	1D χ^2/ν
B^+	A	9.2 ± 3.3	10.6 ± 4.8	12.7/12	6.5/20
	B	9.2 ± 2.9	0.	17.4/13	15.0/17
	C	0.	10.0 ± 4.8	20.7/13	19.3/19
	D	0.	0.	26.4/14	34.2/18
$B^0 + B^+$	A	7.3 ± 3.8	12.0 ± 4.9	8.5/12	15.9/19

and N_{exp}^i are the data and MC simulation event yields, respectively. Indicating with n the number of free parameters, corresponding to the number of resonances included in the fit, the number of degrees of freedom is $\nu = N_{\text{cells}} - n$. In computing the 1D χ^2 we rebin the $J/\psi\phi$ mass projection into 25 bins, again with at least 7 entries per bin.

We perform the fits using models with two resonances (labeled as model A), one resonance (models B and C), and no resonances (model D). The fit projections for fit A are displayed in Fig. 6, showing enhancements with a statistical significance smaller than 3.2σ for all fit models. All models provide a reasonably good description of the data, with χ^2 probability larger than 1%.

We estimate systematic uncertainties on the fractions by varying the mass and the width values for both resonances within their uncertainties. The results shown in Table III are corrected by the fraction of background estimated in each sample. This results in correction factors of 1.12 and 1.21 for the B^+ and the B^0 channels, respectively. We obtain the following background-corrected fractions for B^+ :

$$\begin{aligned} f_{X(4140)} &= (9.2 \pm 3.3 \pm 4.7)\%, \\ f_{X(4270)} &= (10.6 \pm 4.8 \pm 7.1)\%. \end{aligned} \quad (5)$$

Combining statistical and systematic uncertainties in quadrature, we obtain significances of 1.6σ and 1.2σ for the $X(4140)$ and the $X(4270)$, respectively.

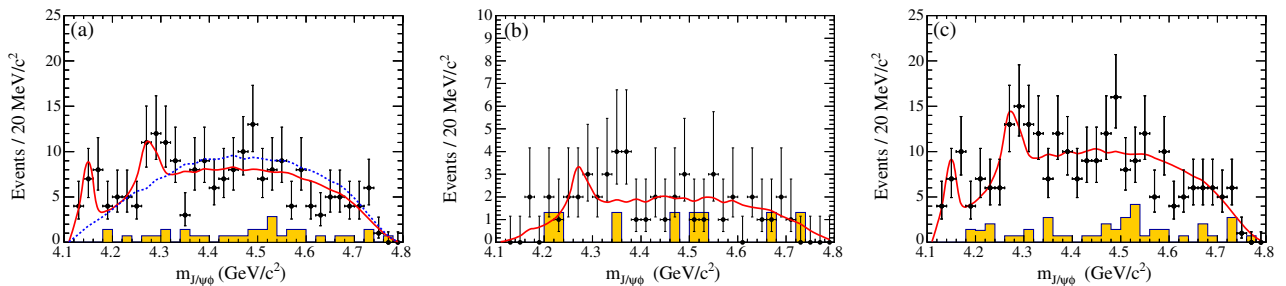


FIG. 7 (color online). Projections on the $J/\psi\phi$ mass spectrum from the Dalitz plot fit with the $X(4140)$ and the $X(4270)$ resonances for the (a) B^+ , (b) B^0 , and (c) combined B^+ and B^0 data samples. The continuous (red) curves result from the fit; the dashed (blue) curve in (a) indicates the projection for fit model D, with no resonances. The shaded (yellow) histograms show the background contributions estimated from the ΔE sidebands.

Using the Feldman-Cousins method [17], we obtain the ULs at 90% C.L.:

$$\begin{aligned} &\mathcal{B}(B^+ \rightarrow X(4140)K^+) \times \mathcal{B}(X(4140) \rightarrow J/\psi\phi) / \\ &\mathcal{B}(B^+ \rightarrow J/\psi\phi K^+) < 0.133, \end{aligned} \quad (6)$$

$$\begin{aligned} &\mathcal{B}(B^+ \rightarrow X(4270)K^+) \times \mathcal{B}(X(4270) \rightarrow J/\psi\phi) / \\ &\mathcal{B}(B^+ \rightarrow J/\psi\phi K^+) < 0.181. \end{aligned} \quad (7)$$

The Feldman-Cousin intervals are evaluated as explained in Ref. [17] and in Sec. III. The $X(4140)$ limit may be compared with the CDF measurement of $0.149 \pm 0.039 \pm 0.024$ [4] and the LHCb limit of 0.07 [6]. The $X(4270)$ limit may be compared with the LHCb limit of 0.08.

The fit projections on the $J/\psi\phi$ mass spectrum using fit model A with two resonances are shown in Fig. 7(a) for B^+ , in Fig. 7(b) for B^0 , and in Fig. 7(c) for the combined B^+ and B^0 sample. The fit results are summarized in Table III.

The central values of mass and width of the two resonances are also fixed to the values recently published by the CMS Collaboration [8]. In this case we obtain, for the B^+ data, the following background-corrected fractions:

$$\begin{aligned} f_{X(4140)} &= (13.2 \pm 3.8 \pm 6.8)\%, \\ f_{X(4270)} &= (10.9 \pm 5.2 \pm 7.3)\%. \end{aligned} \quad (8)$$

These values are consistent within the uncertainties with those obtained in Eq. (5). For comparison, CMS reported a fraction of 0.10 ± 0.03 for the $X(4140)$, which is compatible with the CDF, the LHCb and our value within the uncertainties; CMS could not determine reliably the significance of the second structure, the $X(4270)$, due to possible reflections of two-body decays.

Figure 8(a) shows the efficiency as a function of the $J/\psi\phi$ mass, obtained from a PHSP simulation of the $B^+ \rightarrow J/\psi\phi K^+$ Dalitz plot. We observe a decrease of the efficiency in the $J/\psi\phi$ threshold region, as already observed in Fig. 4.

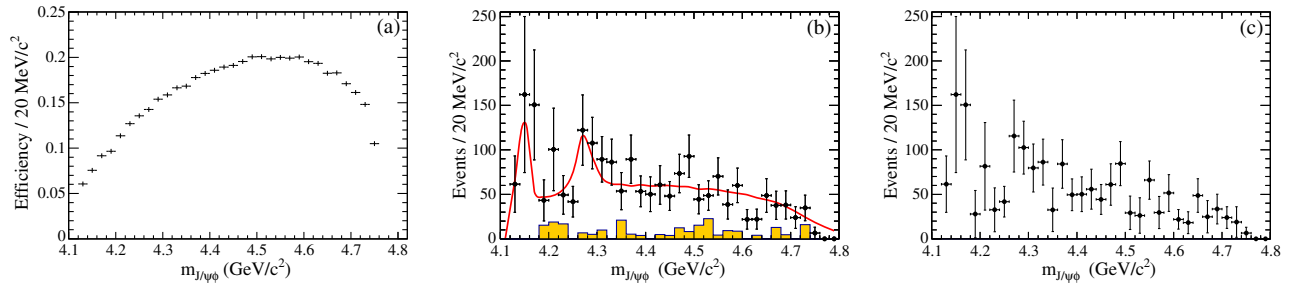


FIG. 8 (color online). (a) Average efficiency distribution as a function of $J/\psi\phi$ invariant mass for $B^+ \rightarrow J/\psi\phi K^+$. (b) Efficiency-corrected $J/\psi\phi$ mass spectrum for the combined B^+ and B^0 samples. The curve is the result from fit model A described in the text. The shaded (yellow) histogram represents the efficiency-corrected background contribution. (c) Efficiency-corrected and background-subtracted $J/\psi\phi$ mass spectrum for the combined B^+ and B^0 samples.

Figure 8(b) shows the efficiency-corrected $J/\psi\phi$ mass spectrum for the combined B^+ and B^0 samples. To obtain this spectrum, we weight each event by the inverse of the efficiency evaluated on the respective B^+ and B^0 Dalitz plot. The curve is the result from fit model A. The background contribution (shown shaded) is estimated from the ΔE sidebands, and has also been corrected for efficiency. However, a few background events fall outside the efficiency Dalitz plots, and to these we assign the same efficiency as for B signal events.

Finally, Fig. 8(c) shows the efficiency-corrected and background-subtracted $J/\psi\phi$ mass spectrum for the combined B^+ and B^0 samples.

V. SUMMARY

In summary, we perform a study of the decays $B^{+,0} \rightarrow J/\psi K^+ K^- K^{+,0}$ and $B^{+,0} \rightarrow J/\psi\phi K^{+,0}$, and for the latter obtain much-improved BF measurements. For $B^+ \rightarrow J/\psi K^+ K^- K^+$, this is the first measurement. We search for resonance production in the $J/\psi\phi$ mass spectrum and obtain significances below 2σ for both the $X(4140)$ and the $X(4270)$ resonances, with systematic uncertainties taken into account. Limits on the product branching ratio values for these resonances are obtained. We find that the hypothesis that the events are distributed uniformly on the Dalitz plot gives a poorer description of the data. We also search for $B^0 \rightarrow J/\psi\phi$ and derive an UL on the BF for

this decay mode, which is in agreement with theoretical expectations.

ACKNOWLEDGMENTS

We are grateful for the extraordinary contributions of our PEP-II2 colleagues in achieving the excellent luminosity and machine conditions that have made this work possible. The success of this project also relies critically on the expertise and dedication of the computing organizations that support *BABAR*. The collaborating institutions wish to thank SLAC for its support and the kind hospitality extended to them. This work is supported by the U.S. Department of Energy and National Science Foundation, the Natural Sciences and Engineering Research Council (Canada), the Commissariat à l’Energie Atomique and Institut National de Physique Nucléaire et de Physique des Particules (France), the Bundesministerium für Bildung und Forschung and Deutsche Forschungsgemeinschaft (Germany), the Istituto Nazionale di Fisica Nucleare (Italy), the Foundation for Fundamental Research on Matter (Netherlands), the Research Council of Norway, the Ministry of Education and Science of the Russian Federation, Ministerio de Ciencia e Innovación (Spain), and the Science and Technology Facilities Council (United Kingdom). Individuals have received support from the Marie-Curie IEF program (European Union), the A. P. Sloan Foundation (USA), and the Binational Science Foundation (USA-Israel).

-
- [1] N. Brambilla *et al.* (Quarkonium Working Group), *Yellow Report*, arXiv:hep-ph/0412158v2; arXiv:1404.3723v2.
 [2] N. Brambilla *et al.*, *Eur. Phys. J. C* **71**, 1534 (2011).
 [3] The use of charge conjugate reactions is implied throughout this work.
 [4] T. Aaltonen *et al.* (CDF Collaboration), *Phys. Rev. Lett.* **102**, 242002 (2009).

- [5] T. Aaltonen *et al.* (CDF Collaboration), arXiv:1101.6058.
 [6] R. Aaij *et al.* (LHCb Collaboration), *Phys. Rev. D* **85**, 091103(R) (2012).
 [7] V. M. Abazov *et al.* (D0 Collaboration), *Phys. Rev. D* **89**, 012004 (2014).
 [8] S. Chatrchyan *et al.* (CMS Collaboration), *Phys. Lett. B* **734**, 261 (2014).

- [9] J. P. Lees *et al.* (BABAR Collaboration), *Nucl. Instrum. Methods Phys. Res., Sect. A* **726**, 203 (2013).
- [10] B. Aubert *et al.* (BABAR Collaboration), *Nucl. Instrum. Methods Phys. Res., Sect. A* **479**, 1 (2002); **729**, 615 (2013).
- [11] J. Beringer *et al.* (PDG Collaboration), *Phys. Rev. D* **86**, 010001 (2012).
- [12] The BF's are calculated by dividing the efficiency-corrected yields in Table I by the product of $N_{BB} \times \prod_i \text{BFS}_i$, where $\text{BFS}_i = \text{BF}$ of particles involved in the relevant $\Upsilon(4S)$ decay and in the corresponding B meson decay processes.
- [13] H. Albrecht *et al.* (ARGUS Collaboration), *Z. Phys. C* **48**, 543 (1990).
- [14] B. Aubert *et al.* (BABAR Collaboration), *Phys. Rev. Lett.* **91**, 071801 (2003).
- [15] A. Anastassov *et al.* (CLEO Collaboration), *Phys. Rev. Lett.* **84**, 1393 (2000).
- [16] R. Aaij *et al.* (LHCb Collaboration), *J. High Energy Phys.* **07** (2014) 140.
- [17] G. J. Feldman and R. D. Cousins, *Phys. Rev. D* **57**, 3873 (1998).
- [18] Y. Liu *et al.* (Belle Collaboration), *Phys. Rev. D* **78**, 011106 (2008).
- [19] R. Aaij *et al.* (LHCb Collaboration), *Phys. Rev. D* **88**, 072005 (2013).